Experiments in Fluids [Suppl.] S166–S174 © Springer-Verlag 2000

Out-of-focus effects on particle image visibility and correlation in microscopic particle image velocimetry

M. G. Olsen, R. J. Adrian

Abstract In microscopic particle image velocimetry (μPIV) the entire volume of a flowfield is illuminated, resulting in all of the particles in the field of view contributing to the image, either by forming discrete particle images or contributing to a background glow. The theory of PIV is expanded to encompass this situation. Equations are derived for a particle image intensity function that yields image diameter and intensity as a function of distance from the object plane, as well as an equation for a new quantity, termed particle visibility. The effect of changing experimental parameters is discussed. Next, the contribution of out-of-focus particles to the correlation function is addressed. A weighting function that can be used to calculate either velocity measurement bias or the distance from the object plane beyond which particles no longer significantly contribute to the correlation function is derived. A new experimental parameter, the depth of correlation, is then introduced, and its dependence on experimental parameters is discussed.

1 Introduction

Particle image velocimetry (PIV) is a well-developed technique used to obtain instantaneous velocity fields (Adrian 1986a, b, 1991). In a typical PIV experiment, small tracer particles are illuminated by a double-pulsed sheet of light, and the images of these particles are captured using either a CCD camera or photographic film. Then, instantaneous velocity fields are determined from the images using a correlation technique. If the depth-of-focus of the camera is made larger than the thickness of the laser sheet, all of the illuminated particles are in focus in the recorded image. Also, the depth over which particle images are captured will be defined by the thickness of the laser sheet.

M. G. Olsen (✉), R. J. Adrian
Beckman Institute for Advanced Science and Technology
University of Illinois at Urbana-Champaign
405 N. Mathews, Urbana, IL 61801, USA

R. J. Adrian
Department of Theoretical and Applied Mechanics
University of Illinois at Urbana-Champaign
104 S. Wright, Urbana, IL 61801, USA

This work was supported by the DARPA/ETO μFlumes and composite CAD programs.

Microscopic particle image velocimetry (μPIV) is a recently developed technique for measuring velocity fields in microfluidic devices (Santiago et al. 1998; Meinhart et al. 1999). A diagram of a μPIV system is presented in Fig. 1. The microfluidic device of interest is placed beneath the objective of an epi-fluorescent microscope. The light beam from a double-pulsed Nd:YAG laser is expanded before entering the microscope through an aperture in the back of the microscope. After being redirected towards the microfluidic device by a prism, the laser light is focused onto a small region of the sample by the microscopic objective.

Because of the small length scales involved in μPIV, it is difficult to illuminate only a small slice of the flowfield with a laser sheet, as is typically done in PIV. Instead, the entire flowfield is illuminated, and the depth over which particle images are obtained is determined by the depth of focus of the microscope objective, not the thickness of a laser sheet. One consequence of this method of illumination is that both the light from the illuminating laser beam reflected by the test section and the light from the seed particles are directed towards the CCD camera. These two components can be separated by using fluorescent particles and a fluorescence filter cube. Because the particles fluoresce at a longer wavelength than the illuminating laser light, by choosing the proper filter cube, the laser light can be removed, while the light from the particles still reaches the CCD camera.

Volume illumination is not unique to μPIV. Volume illumination is also used in creating the holographic plates used in holographic PIV (Barnhart et al. 1994; Meng and Hussain 1995). However, there is a significant difference in the interrogation of holographic PIV images and the interrogation of μPIV images. In interrogating a hologram, a coherent light source is used. Because of this, the scattered light from the out-of-focus particles will form speckle patterns. In μPIV, however, the light from the particles is emitted and not scattered light; hence, the light is incoherent, and there will be no resulting speckle pattern.

The work presented here addresses several issues arising from illuminating the entire volume of the flowfield, as is done in μPIV. These issues include the variation in particle image intensity and diameter as a function of distance from the focal plane, the visibility of particles over the background glow created by particles far from the focal plane, the contribution to the correlation function of particles outside the focal plane, and the biasing of velocity measurements due to out-of-focus particles. The effect

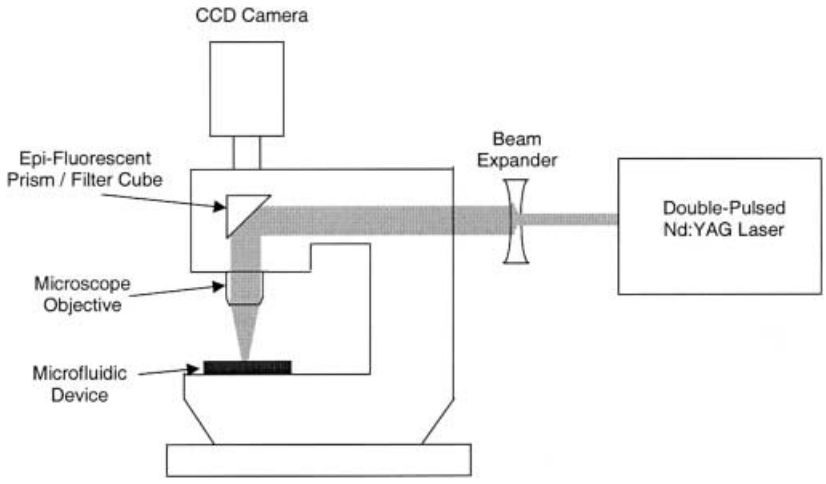

Fig. 1. Diagram of a microscope-based μPIV system

of various experimental parameters on each of these phenomena is also discussed.

2
Image plane intensity distribution

In deriving a model for the image plane intensity distribution of the fluorescent seed particles, several key assumptions are made. The first is that all the seed particles have the same diameter. This is a reasonable assumption, since fluorescent seed particles are readily available with a root mean square variation in diameter of less than 5%. It is further assumed that the entire field of view is illuminated with equal laser intensity. Finally, the fluorescent particles are assumed to emit light isotropically. If it is assumed that the fluorescent particles are all illuminated equally and are of identical diameter, it follows that all the particles emit an equal amount of light. Because the illuminating light from the laser is filtered out, only light from the fluorescing particles reaches the CCD camera.

In light-sheet PIV with the proper selection of optics, only in-focus particles are illuminated. In μPIV, however, all the particles in the flowfield are illuminated, and the images of the particles vary based on their location in the microfluidic device. An equation describing the change in particle image diameter and intensity as a function of distance from the object plane must be derived. The optical geometry used in deriving this equation is shown in Fig. 2.

The diameter of the image formed by a particle located in the object plane (and thus in perfect focus) can be estimated by (Adrian and Yao 1983)

$$d_e = (M^2 d_p^2 + d_s^2)^{1/2} \tag{1}$$

with

$$d_s = 2.44(M+1)\lambda f^{\#} \tag{2}$$

equal to the diameter of the point response function of a diffraction-limited lens measured at the first dark ring of the Airy disk intensity distribution. In this equation, M is the magnification, d_p is the particle diameter, λ is the wavelength of light emitted by the particle, and $f^{\#}$ is the focal number of the lens. (In microscopy, the numerical aperture, NA $= 1/2f^{\#}$, is often used instead of $f^{\#}$.) Equation (1) represents the combined effects of magnifying the geometric image of the particle and diffraction. It is an approximation obtained by modeling both the Airy function and the geometric image as Gaussian functions. If the point response function and the geometric optics contribution are both Gaussian, then Eq. (1) is exact. Adrian and Yao (1985) demonstrated that a Gaussian distribution is a good approximation to the Airy distribution.

As the particle moves away from the image plane, the geometric optics term increases due to spreading of the image. Incorporating this spreading of the geometrics optics term into Eq. (1) results in

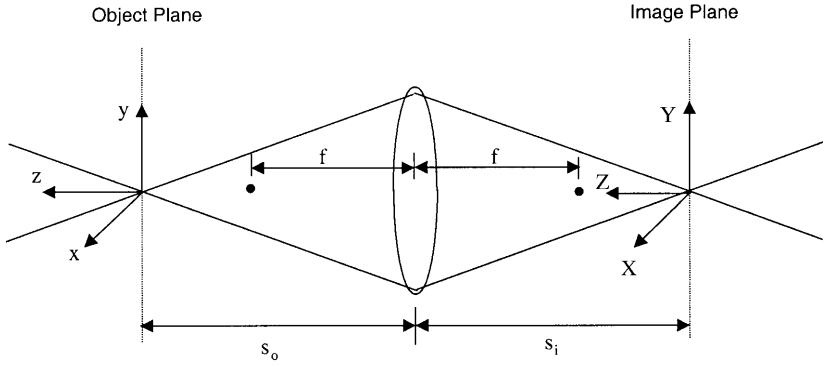

Fig. 2. Optical geometry used in deriving the particle image intensity model

$$d_e(z) = \left(M^2 d_p^2 + 5.95(M+1)^2 \lambda^2 f^{\#2} + \frac{M^2 z^2 D_a^2}{(s_o + z)^2} \right)^{1/2} \quad (3)$$

where D_a is the lens aperture diameter. Equation (3) assumes that both the geometric optics term and the diffraction term can be approximated as Gaussian. In any microscopic measurement, $s_o \gg z$, and the image diameter grows as $d_e \propto (\text{const.} + z^2)^{1/2}$, which is a hyperbola.

The amount of light from a particle reaching the image plane depends on the solid angle the lens subtends. The flux of the light from a particle that reaches the image plane can be expressed as

$$J = \frac{J_p D_a^2}{16(s_o + z)^2} \quad (4)$$

where J_p is the flux of light emitted from the particle surface and is dependent on the illumination received by the particle.

If the distribution of light intensity in the particle image is assumed to be Gaussian, and if the edge of the image is defined as occurring at $\exp(-\beta^2)$, then the distribution can be expressed as $I = I_o \exp(-4\beta^2 r^2 / d_i^2)$. The constant I_o can be solved for by noting that the integrated intensity over the particle image must be equal to the power of light from the particle reaching the image plane. This leads to the result

$$I(r,z) = \frac{J_p D_a^2 \beta^2}{4\pi d_e^2 (s_o + z)^2} \exp\left(\frac{-4\beta^2 r^2}{d_e^2} \right) \quad (5)$$

Adrian and Yao (1985) found that for the Gaussian distribution to best approximate an Airy distribution, $\beta^2 = 3.67$.

The accuracy of this model in predicting the dependence of peak particle image intensity with z distance from the object plane has been determined experimentally. Fluorescent particles measuring 1.06 μm in diameter were placed on a slide and observed under the microscope with a 20×, NA = 0.5 objective. The images of these particles were then recorded using a 12-bit CCD camera at various distances from the object plane. The particle images were then analyzed to determine image intensity at the center of the particle image, as this is where the image intensity peaks.

Figure 3 is a comparison of the experimentally determined dependency of peak particle image intensity $I(0,z)/I(0,0)$ with the relationship derived in Eq. (5). Both have been normalized by the peak image intensity at $z = 0$. The model slightly underpredicts the peak particle image intensity, but the agreement is good enough for the present purpose.

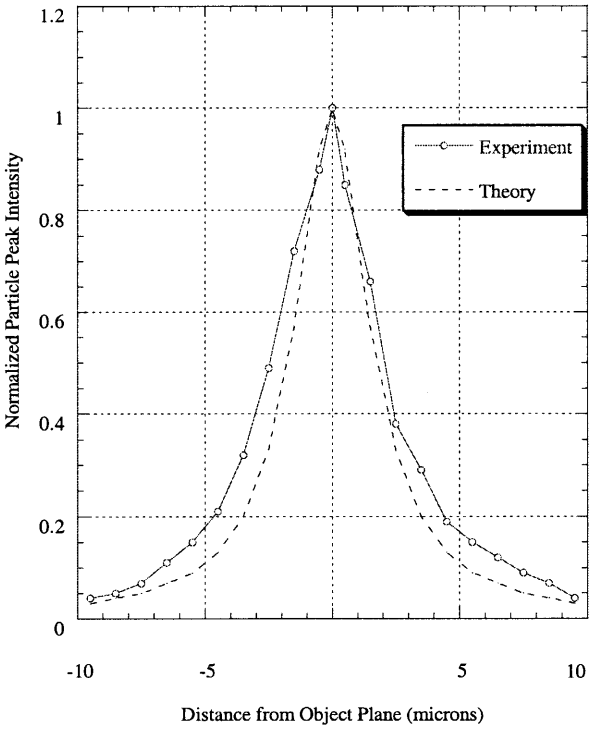

Fig. 3. Comparison of theoretical with experimental results for particle image intensity

3 Particle visibility

The fact that all the particles in the field of view contribute to the image is a major problem in μPIV. The light from particles far from the object plane forms a background glow that can make it difficult to see the in-focus particles. To evaluate the effect of out-of-focus particles, we consider a channel, as shown in Fig. 4. The object plane is located a distance a from the top of the channel, which has a depth of L.

The particles in the channel are divided into two groups. Group 1 contains the particles that are bright enough to be seen above the background glow. These particles are located in the region defined by depth δ. Group 2 contains the particles contributing to the background glow. If C is the particle concentration (with units of particles/μm^3), and if $L \ll s_o$, then the number of particles contributing to the background glow is

$$N_p = (L - \delta) A_v C \quad (6)$$

The total flux of background light from the particles is

$$J_B = \int_{-a}^{-\delta/2} \frac{C J_p D_a^2}{16(s_o + z)^2} \, dx \, dy \, dz + \int_{\delta/2}^{L-a} \frac{C J_p D_a^2}{16(s_o + z)^2} \, dx \, dy \, dz \quad (7)$$

Assuming that $s_o \gg \delta/2$, and uniform properties within the field of view, the solution to this integral becomes

$$J_B = \frac{C J_p L D_a^2 A_v}{16(s_o - a)(s_o - a + L)} \quad (8)$$

If this flux is evenly distributed over the entire area of view in the image plane, the intensity of the background glow in the image can be expressed as

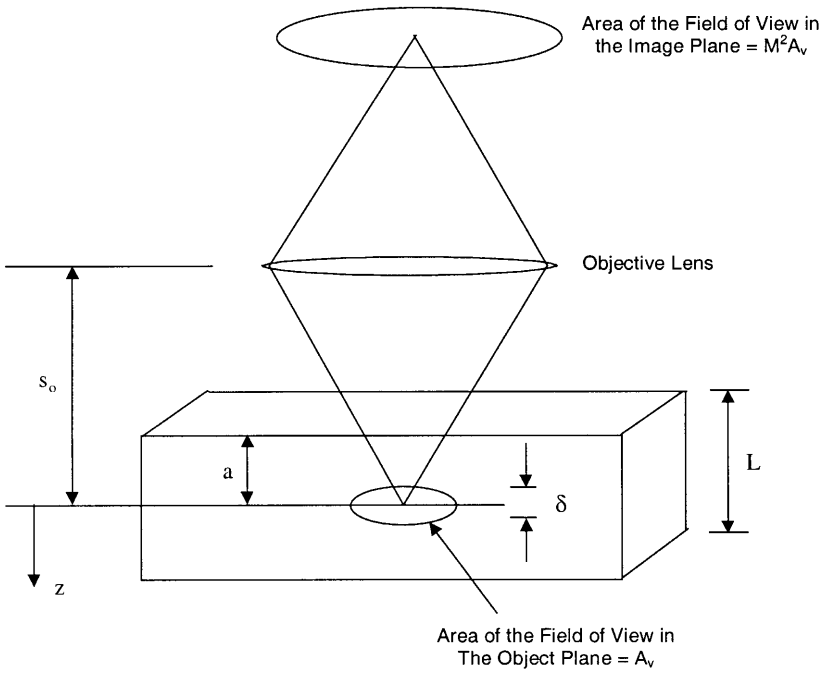

Fig. 4. Channel geometry used in deriving the particle visibility

$$I_B = \frac{CJ_pLD_a^2}{16M^2(s_o - a)(s_o - a + L)} \tag{9}$$

This is the mean intensity of the background glow. Fluctuations in the intensity of the background glow are not considered in this analysis. The particles in group 1 are visible only if their peak intensities rise significantly above the background glow. The peak intensity of a particle image occurs at $r = 0$ (the center of a particle image), thus for a particle to be visible, one must have

$$I(0,z) = \frac{J_pD_a^2\beta^2}{4\pi d_e^2(s_o + z)^2} > \frac{\gamma CJ_pLD_a^2}{16M^2(s_o - a)(s_o - a + L)} \tag{10}$$

where γ is the percentage of the background glow intensity that a particle image's peak intensity must be to be seen over the background glow. This parameter depends on the sensitivity of the CCD camera used.

After substituting Eq. (3) for d_e into Eq. (10), assuming that $s_o \gg z$, and noting that at high magnification, $f^{\#} \cong s_o/D_a$, the following inequality is derived

$$z < \left[\frac{4\beta^2(s_o - a)(s_o - a + L)}{4\pi D_a^2 CL} - \frac{M^2f^{\#2}d_p^2 + 5.95(M+1)^2\lambda^2f^{\#4}}{M^2}\right]^{1/2} = z_{max} \tag{11}$$

This inequality gives the maximum z distance a particle can be from the object plane and still be visible over the background glow as a function of various experimental parameters.

Depending on the circumstances, it may be desirable to either minimize or maximize z_{max}. For example, if strong velocity gradients exist in the z direction, then it would be desirable to minimize z_{max} and thus reduce biasing of velocity measurements due to particles far from the focal plane. If adequately seeding the flow is a problem, then it may be desirable to increase z_{max}. z_{max} becomes zero when even the brightest (i.e., most sharply focused) particles no longer can be detected above the background glow. This defines the maximum useful concentration.

Note that in μPIV applications magnification is likely to be high, and $M + 1 \cong M$. This results in z_{max} being very weakly dependent on magnification. The effect of $f^{\#}$ on z_{max} can be seen by assuming that $\frac{(s_o-a)(s_o-a+L)}{D_a^2} \cong f^{\#2}$, resulting in the approximation

$$z_{max} \cong f^{\#}\left[\frac{4\beta^2}{\gamma\pi CL} - \frac{M^2d_p^2 + 5.95(M+1)^2\lambda^2f^{\#2}}{M^2}\right]^{1/2} \tag{12}$$

Thus, z_{max} increases approximately linearly with $f^{\#}$, especially for large particles.

If all of the optical parameters are kept constant, z_{max} can be increased by decreasing either the particle concentration or the depth of the device. Decreasing either of these parameters has the effect of decreasing the intensity of the background glow. Also, increasing a, the distance of the object plane from the top of the channel will reduce z_{max}. This is because when a is small, the bulk of the out-of-focus particles are farther from the microscope objective than when a is large, and thus less of their light is collected by the objective reducing the intensity of the background glow.

Finally, the *visibility* of a particle can be defined as the ratio of the peak intensity of the in-focus particle image to the intensity of the background glow, namely

$$V = \frac{4M^2\beta^2(s_o - a)(s_o - a + L)}{\pi CL\left[(s_o + z)^2\left(M^2d_p^2 + 5.95(M+1)^2\lambda^2f^{\#2}\right) + M^2z^2D_a^2\right]} \tag{13}$$

The peak in visibility will occur at $z = 0$, where the particles are in perfect focus. The peak visibility is given by

$$V_{\text{peak}} = \frac{4M^2\beta^2(s_o - a)(s_o - a + L)}{\pi CLs_o^2\left(M^2 d_p^2 + 5.95(M+1)^2\lambda^2 f^{\#2}\right)} \tag{14}$$

Particle visibility is only weakly dependent on magnification, and can be most readily increased by decreasing the $f^{\#}$ of the optical system. If the optical parameters are kept constant, then particle visibility can be increased by either decreasing the depth of the device being imaged or using a lower particle concentration. However, using a lower particle concentration will have the additional effect of reducing the number of particles within each interrogation volume. This will result in noisier velocity estimates and possibly necessitate using larger interrogation spots, resulting in lower spatial resolution.

Meinhart et al. (1999) have been able to maintain high spatial resolution at low particle concentration by taking many realizations and then averaging the calculated spatial correlations for each interrogation region to yield a single high-vector-density velocity field. However, this technique is limited to steady flows or periodic flows with phase-locking.

4 Effects on the correlation function

4.1 Components of the correlation function

A very important consideration in μPIV is the effect that out-of-focus particles have on the correlation function and any velocity biasing effects that they might cause. In analyzing the effect of out-of-focus particles on the correlation function, consider the experimental geometry shown in Fig. 5. All particles in the interrogation volume of diameter d_I contribute to the interrogation spot image of diameter $Md_I = D_I$. Ideally, one would like only those particles within a short distance of the object plane to contribute significantly to the correlation function. The measured velocity vector will actually be a volume-averaged vector, so the longer the distance from the object plane that particles significantly contribute to the correlation function, the greater the depth over which the measured velocity vector is averaged.

If the analysis is done by cross-correlation analysis, two images are taken of the flowfield at times t_1 and $t_2 = t_1 + \Delta t$. Assuming that the background glow is uniform, and it is subtracted from the images, then, following the analyses of Keane and Adrian (1990, 1991, 1992) the two images to be cross correlated can be defined as $I_1(\mathbf{X})$ and $I_2(\mathbf{X})$, such that

$$I_1(\mathbf{X}) = W_{I1}(\mathbf{X} - \mathbf{X}_1)\int I_{o1}(\mathbf{x})\hat{J}_o[\mathbf{X} - M(x,y); z]g(\mathbf{x}, t_1)\mathrm{d}\mathbf{x} \tag{15}$$

$$I_2(\mathbf{X}) = W_{I2}(\mathbf{X} - \mathbf{X}_2)\int I_{o2}(\mathbf{x}')\hat{J}_o[\mathbf{X} - M(x',y'); z']g(\mathbf{x}', t_2)\mathrm{d}\mathbf{x}' \tag{16}$$

where W_{Ii} are weighting functions which define the interrogation windows, I_{oi} define the illumination pulses, $\hat{J}_o$ is the particle image intensity function per unit of intensity that illuminates a particle located at $\mathbf{x}$ in the flowfield, and

$$g(\mathbf{x}, t) = \sum_i \delta(\mathbf{x} - \mathbf{x}_i(t)) \tag{17}$$

indicates the Lagrangian position $\mathbf{x}_i(t)$ of each particle in the flow at time t. Thus, I_1 and I_2 are the convolutions of the illuminating pulses and the particle image intensity function with the positions of the particles in the flowfield at times t_1 and t_2.

The spatial cross-correlation of the two images can be approximated by a convolution

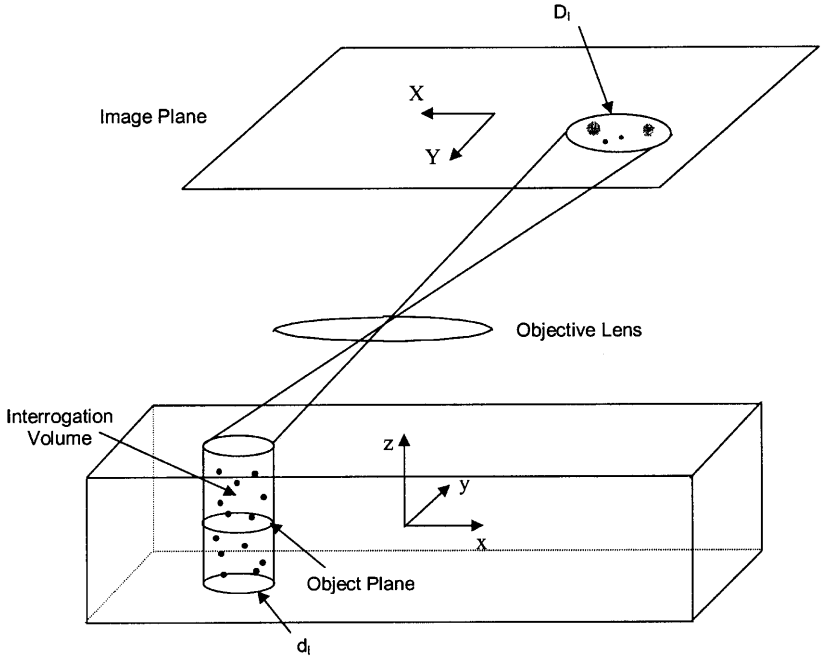

Fig. 5. Geometry for determining the effect of out-of-focus particle on the correlation function

$$R(\mathbf{s}) = \int I_1(\mathbf{X}) I_2(\mathbf{X}+\mathbf{s}) \mathrm{d}\mathbf{X} \tag{18}$$

It proves convenient to decompose $g(\mathbf{x}, t)$ into mean and fluctuating parts, such that

$$g(\mathbf{x}, t) = C(\mathbf{x}, t) + \Delta g(\mathbf{x}, t) \tag{19}$$

where the mean of g is simply the local mean concentration

$$\langle g(\mathbf{x}, t) \rangle = C(\mathbf{x}, t) \tag{20}$$

Thus $\langle \Delta g(\mathbf{x}, t) \rangle = 0$. Now, substitute Eqs. (15), (16), (19), and (20) into (18) to get

$$\begin{aligned} R(\mathbf{s}) = \int \mathrm{d}\mathbf{X} \int & W_{\mathrm{I}1}(\mathbf{X}-\mathbf{X_1})(C(\mathbf{x}, t_1) \\ & + \Delta g(\mathbf{x}, t_1)) I_{\mathrm{o}1}(\mathbf{x}) \hat{J}_{\mathrm{o}}[\mathbf{X} - M(x, y); z] \mathrm{d}\mathbf{x} \\ & \times \int W_{\mathrm{I}2}(\mathbf{X}-\mathbf{X_2}+\mathbf{s})(C(\mathbf{x}', t_2) \\ & + \Delta g(\mathbf{x}', t_2)) I_{\mathrm{o}2}(\mathbf{x}') \hat{J}_{\mathrm{o}}[\mathbf{X} - M(x', y') + \mathbf{s}; z'] \mathrm{d}\mathbf{x}' \end{aligned} \tag{21}$$

$R(\mathbf{s})$ can be decomposed into three components, such that

$$R(\mathbf{s}) = R_{\mathrm{C}}(\mathbf{s}) + R_{\mathrm{F}}(\mathbf{s}) + R_{\mathrm{D}}(\mathbf{s}) \tag{22}$$

$R_{\mathrm{C}}(\mathbf{s})$ is the convolution of the mean intensities. It is a broad function of $\mathbf{s}$ with a diameter of order d_{I}, and it is given by

$$\begin{aligned} R_{\mathrm{C}}(\mathbf{s}) = \int \mathrm{d}\mathbf{X} \int & W_{\mathrm{I}1}(\mathbf{X}-\mathbf{X}_1) C(\mathbf{x}, t_1) I_{\mathrm{o}1}(\mathbf{x}) \\ & \times \hat{J}_{\mathrm{o}}[\mathbf{X} - M(x, y); z] \mathrm{d}\mathbf{x} \\ & \times \int W_{\mathrm{I}2}(\mathbf{X}-\mathbf{X}_2+\mathbf{s}) C(\mathbf{x}', t_2) I_{\mathrm{o}2}(\mathbf{x}') \\ & \times \hat{J}_{\mathrm{o}}[\mathbf{X} - M(x', y') + \mathbf{s}; z'] \mathrm{d}\mathbf{x}' \end{aligned} \tag{23}$$

$R_{\mathrm{F}}(\mathbf{s})$ is the fluctuating noise component, and it is given by

$$\begin{aligned} R_{\mathrm{F}}(\mathbf{s}) = \int \mathrm{d}\mathbf{X} \int & W_{\mathrm{I}1}(\mathbf{X}-\mathbf{X}_1) C(\mathbf{x}, t_1) I_{\mathrm{o}1}(\mathbf{x}) \\ & \times \hat{J}_{\mathrm{o}}[\mathbf{X} - M(x, y); z] \mathrm{d}\mathbf{x} \\ & \times \int W_{\mathrm{I}2}(\mathbf{X}-\mathbf{X}_2+\mathbf{s}) \Delta g(\mathbf{x}', t_2) I_{\mathrm{o}2}(x') \\ & \times \hat{J}_{\mathrm{o}}[\mathbf{X} - M(x', y') + \mathbf{s}; z'] \mathrm{d}\mathbf{x}' \\ & + \int \mathrm{d}\mathbf{X} \int W_{\mathrm{I}1}(\mathbf{X}-\mathbf{X}_1) \Delta g(\mathbf{x}, t_1) I_{\mathrm{o}1}(x) \\ & \times \hat{J}_{\mathrm{o}}[\mathbf{X} - M(x, y); z] \mathrm{d}\mathbf{x} \\ & \times \int W_{\mathrm{I}2}(\mathbf{X}-\mathbf{X}_2+\mathbf{s}) C(\mathbf{x}', t_2) I_{\mathrm{o}2}(\mathbf{x}') \\ & \times \hat{J}_{\mathrm{o}}[\mathbf{X} - M(x', y') + \mathbf{s}; z'] \mathrm{d}\mathbf{x}' \end{aligned} \tag{24}$$

$R_{\mathrm{D}}(\mathbf{s})$ is the displacement component of the correlation function. It gives the image displacement from time t_1 to t_2.

$$\begin{aligned} R_{\mathrm{D}}(\mathbf{s}) = \int \mathrm{d}\mathbf{X} \int & W_{\mathrm{I}1}(\mathbf{X}-\mathbf{X}_1) \Delta g(\mathbf{x}, t_1) I_{\mathrm{o}1}(\mathbf{x}) \\ & \times \hat{J}_{\mathrm{o}}[\mathbf{X} - M(x, y); z] \mathrm{d}\mathbf{x} \\ & \times \int W_{\mathrm{I}2}(\mathbf{X}-\mathbf{X}_2+\mathbf{s}) \Delta g(\mathbf{x}', t_2) I_{\mathrm{o}2}(\mathbf{x}') \\ & \times \hat{J}_{\mathrm{o}}[\mathbf{X} - M(x', y') + \mathbf{s}; z'] \mathrm{d}\mathbf{x}' \end{aligned} \tag{25}$$

4.2 Statistical properties

In any pair of PIV images to be cross correlated, the particle locations are random. This randomness causes variations in the correlation fields even for two interrogation spots with identical fluid velocities. It is therefore appropriate to deal with averages of the correlation fields. Since the velocity fields may also be random, it is convenient to fix the fields by considering $\langle R(\mathbf{s}) | \mathbf{u}(\mathbf{x}, t) \rangle$, the conditional average of $R(\mathbf{s})$ given the velocity field. The conditional average $\langle R(\mathbf{s}) | \mathbf{u}(\mathbf{x}, t) \rangle$, is found by conditionally averaging each term in Eq. (22) and then using the following equation for $\langle \Delta g(\mathbf{x}, t_1) \Delta g(\mathbf{x}', t_2) | u(\mathbf{x}, t) \rangle$ (cf. Adrian 1986b):

$$\begin{aligned} & \langle \Delta g(\mathbf{x}, t_1) \Delta g(\mathbf{x}', t_2) | \mathbf{u}(\mathbf{x}, t) \rangle \\ & \quad = C(\mathbf{x}, t_1) \delta(\mathbf{x}' - \mathbf{x} - \mathbf{u}(\mathbf{x}, t) \Delta t) \end{aligned} \tag{26}$$

This results in

$$\begin{aligned} \langle R_{\mathrm{C}}(\mathbf{s}) | \mathbf{u} \rangle = R_{\mathrm{C}}(\mathbf{s}) = \int \mathrm{d}\mathbf{X} \int & W_{\mathrm{I}1}(\mathbf{X}-\mathbf{X}_1) C(\mathbf{x}, t_1) I_{\mathrm{o}1}(\mathbf{x}) \\ & \times \hat{J}_{\mathrm{o}}[\mathbf{X} - M(x, y); z] \mathrm{d}\mathbf{x} \\ & \times \int W_{\mathrm{I}2}(\mathbf{X}-\mathbf{X}_2+\mathbf{s}) C(\mathbf{x}', t_2) I_{\mathrm{o}2}(\mathbf{x}') \\ & \times \hat{J}_{\mathrm{o}}[\mathbf{X} - M(x', y') + \mathbf{s}; z'] \mathrm{d}\mathbf{x}' \end{aligned} \tag{27}$$

$$\langle R_{\mathrm{F}}(\mathbf{s}) | \mathbf{u} \rangle = 0 \tag{28}$$

$$\begin{aligned} \langle R_{\mathrm{D}}(\mathbf{s}) | \mathbf{u} \rangle = & \int \mathrm{d}\mathbf{X} W_{\mathrm{I}1}(\mathbf{X}-\mathbf{X}_1) W_{\mathrm{I}1}(\mathbf{X}-\mathbf{X}_2+\mathbf{s}) \\ & \times \int \mathrm{d}\mathbf{x} C(\mathbf{x}, t_1) I_{\mathrm{o}1}(\mathbf{x}) I_{\mathrm{o}2}(\mathbf{x}+\Delta\mathbf{x}) \\ & \times \hat{J}_{\mathrm{o}}[\mathbf{X} - M\mathbf{x}; z] \\ & \times \hat{J}_{\mathrm{o}}[\mathbf{X} - M\mathbf{x} - M(\Delta x, \Delta y) + \mathbf{s}; z + \Delta z] \mathrm{d}\mathbf{x} \end{aligned} \tag{29}$$

where $\Delta\mathbf{x} = \mathbf{u}\Delta t$. $\langle R_{\mathrm{C}}(\mathbf{s}) | \mathbf{u} \rangle$ is approximately the convolution of the mean intensity throughout the interrogation spot with itself. If both the particle concentration and image intensity are uniform throughout the interrogation spot, then $\langle R_{\mathrm{C}}(\mathbf{s}) | \mathbf{u} \rangle$ will be the convolution of two constant functions. Otherwise, it is the convolution of two slowly varying functions. In either case, $\langle R_{\mathrm{C}}(\mathbf{s}) | \mathbf{u} \rangle$ is a broad function of $\mathbf{s}$ with a diameter of approximately d_{I}.

$\langle R_{\mathrm{D}}(\mathbf{s}) | \mathbf{u} \rangle$ is the component of the correlation function based on particle displacement from time t_1 to t_2 and, as such, it contains the velocity information for the

interrogation spot. The integrand in Eq. (29) vanishes unless the product of $J_o[\mathbf{X} - M(x,y); z]$ and $J_o[\mathbf{X} - M(x,y) - M(\Delta x, \Delta y) + \mathbf{s}; z + \Delta z]$ is large, requiring that $X \cong M(x,y) \cong M(x,y) + M(\Delta x, \Delta y) - s$ Then, $\langle R_D(\mathbf{s})|\mathbf{u}\rangle$ simplifies to

$$\langle R_D(\mathbf{s})|\mathbf{u}\rangle = \int d\mathbf{x} C(\mathbf{x},t) I_{o1}(\mathbf{x}) I_{o2}(\mathbf{x}+\Delta\mathbf{x}) \times W_{I1}(M\mathbf{x} - \mathbf{X_1}) W_{I2}(M\mathbf{x} + M\Delta\mathbf{x} - \mathbf{X_2}) \times \int d\mathbf{X} \hat{J}_o[\mathbf{X}; z] \hat{J}_o[\mathbf{X} - M(\Delta x, \Delta y) + \mathbf{s}; z + \Delta z] \quad (30)$$

The more common method for measuring the velocity is to locate the point where $\partial R_D/\partial \mathbf{s} = 0$, denoted by $\mathbf{s}_o$. Since the model for the correlation function presented here is continuous, this point is easily found. In a real PIV experiment, where the data are discretized by the CCD camera, this requires first fitting a paraboloid to $\langle R_D(\mathbf{s})|\mathbf{u}\rangle$. The velocity found by this method is

$$\mathbf{u}_o = \frac{\mathbf{s}_o}{M\Delta t} \quad (36)$$

Before setting $(\partial R_D/\partial \mathbf{s})_{\mathbf{s}_0}$ in Eq. (33), first make the assumption that

$$F_\tau[\mathbf{s} - M(\Delta x, \Delta y); z, \Delta z] = \hat{f}\left[|\mathbf{s} - M(\Delta x, \Delta y)|^2;\ z, \Delta z\right]$$

as it would be if the particle images were Gaussian. Then, noting that $\Delta\mathbf{x} = \mathbf{u}\Delta t$, one finds that

$$\mathbf{u_o} = \frac{\int d\mathbf{x} C(\mathbf{x},t) W_{I1}(M\mathbf{x} - \mathbf{X_1}) W_{I2}(M\mathbf{x} + M\Delta\mathbf{x} - \mathbf{X_2}) \left[\int \hat{J}_o d\mathbf{X}\right]^2 \left(\frac{\partial \hat{f}}{\partial |\mathbf{s} - M\mathbf{u}\Delta t|^2}\right)_{\mathbf{s}_o} \mathbf{u}(\mathbf{x},t)}{\int d\mathbf{x} C(\mathbf{x},t) W_{I1}(M\mathbf{x} - \mathbf{X_1}) W_{I2}(M\mathbf{x} + M\Delta\mathbf{x} - \mathbf{X_2}) \left[\int \hat{J}_o d\mathbf{X}\right]^2 \left(\frac{\partial \hat{f}}{\partial |\mathbf{s} - M\mathbf{u}\Delta t|^2}\right)_{\mathbf{s}_o}} \quad (37)$$

which can be written as

$$\langle R_D(\mathbf{s})|\mathbf{u}\rangle = \int d\mathbf{x} C(\mathbf{x},t) I_{o1}(\mathbf{x}) I_{o2}(\mathbf{x}+\Delta\mathbf{x}) \times W_{I1}(M\mathbf{x} - \mathbf{X_1}) W_{I2}(M\mathbf{x} + M\Delta\mathbf{x} - \mathbf{X_2}) \times \left[\int \hat{J}_o d\mathbf{X}\right]^2 F_\tau(\mathbf{s} - M(\Delta x, \Delta y); z, \Delta z) \quad (31)$$

where

$$F_\tau(\mathbf{s}) = \frac{\int \hat{J}_o[\mathbf{X}; z] \hat{J}_o[\mathbf{X} + \mathbf{s}; z + \Delta z] d\mathbf{X}}{\left[\int \hat{J}_o d\mathbf{X}\right]^2} \quad (32)$$

If $I_{o1} = I_{o2} = I_o$ and I_{o1} and I_{o2} are independent of x, y, and z, then Eq. (32) becomes

$$\langle R_D(\mathbf{s})|\mathbf{u}\rangle = I_o^2 \int d\mathbf{x} C(\mathbf{x},t) W_{I1}(M\mathbf{x} - \mathbf{X_1}) \times W_{I2}(M\mathbf{x} + M\Delta\mathbf{x} - \mathbf{X_2}) \left[\int \hat{J}_o d\mathbf{X}\right]^2 \times F_\tau(\mathbf{s} - M(\Delta x, \Delta y); z, \Delta z) \quad (33)$$

where, in general, $\Delta\mathbf{x} = \Delta\mathbf{x}(\mathbf{x})$ and F_τ is narrow.

In PIV, the measured velocity is defined to be the image displacement inferred from the average correlation function divided by $M\Delta t$, i.e., the inferred particle displacement divided by Δt. If the image displacement is determined by finding the centroid of the conditional mean correlation, defined by

$$\mathbf{s}_{cent} = \frac{\int \mathbf{s}\langle R_D(\mathbf{s})|\mathbf{u}\rangle d\mathbf{s}}{\int \langle R_D(\mathbf{s})|\mathbf{u}\rangle d\mathbf{s}} \quad (34)$$

then

$$\mathbf{u}_{cent} = \frac{\mathbf{s}_{cent}}{M\Delta t} = \frac{1}{M\Delta t} \frac{\int d\mathbf{x} C(\mathbf{x},t) W_{I1}(M\mathbf{x} - \mathbf{X_1}) W_{I2}(M\mathbf{x} + M\Delta\mathbf{x} - \mathbf{X_2}) \left[\int \hat{J}_o d\mathbf{X}\right]^2 \int \mathbf{s} F_\tau d\mathbf{s}}{\int d\mathbf{x} C(\mathbf{x},t) W_{I1}(M\mathbf{x} - \mathbf{X_1}) W_{I2}(M\mathbf{x} + M\Delta\mathbf{x} - \mathbf{X_2}) \left[\int \hat{J}_o d\mathbf{X}\right]^2 \int F_\tau d\mathbf{s}} \quad (35)$$

Equation (37) is implicit in $\mathbf{u}(\mathbf{x},t)$ in that $\mathbf{u}$ appears in both sides of the equation, and as such, $\mathbf{u}_o$ is an approximation of $\mathbf{u}(\mathbf{x}, t)$. However, although $\mathbf{u}(\mathbf{x})$ varies within the interrogation volume, as long as the variation is not too great, then $\mathbf{s} - M\mathbf{u}(\mathbf{x})\Delta t \cong 0$, and the exponential term in both the top and bottom of Eq. (37) will be approximately equal to 1. Using this approximation, Eq. (37) can be written as

$$\mathbf{u_o} = \frac{\int d\mathbf{x} C(\mathbf{x},t) W_{I1}(M\mathbf{x} - \mathbf{X_1}) W_{I2}(M\mathbf{x} + M\Delta\mathbf{x} - \mathbf{X_2}) \left[\int \hat{J}_o d\mathbf{X}\right]^2 \mathbf{u}(\mathbf{x},t)}{\int d\mathbf{x} C(\mathbf{x},t) W_{I1}(M\mathbf{x} - \mathbf{X_1}) W_{I2}(M\mathbf{x} + M\Delta\mathbf{x} - \mathbf{X_2}) \left[\int \hat{J}_o d\mathbf{X}\right]^2} \quad (38)$$

or

$$\mathbf{u_o} = \frac{\int \mathbf{u}(\mathbf{x},t) W(\mathbf{x}) d\mathbf{x}}{\int W(\mathbf{x}) d\mathbf{x}} \quad (39)$$

where $W(\mathbf{x})$ is the weighting function

$$W(\mathbf{x}) = C(\mathbf{x},t) W_{I1}(M\mathbf{x} - \mathbf{X_1}) \times W_{I2}(M\mathbf{x} + M\Delta\mathbf{x} - \mathbf{X_2}) \left[\int \hat{J}_o d\mathbf{X}\right]^2 \quad (40)$$

This weighting function gives the relative contribution to the correlation function as a function of position. Since it depends on $\Delta\mathbf{x}$, there is a bias of the measured velocity due to velocity variation within the interrogation volume. This bias due to variation in the (X, Y) plane can be reduced by making W_{I2} flat and wide compared with W_{I1}. Biases due to variation in z are not removed so easily.

4.3
Approximate model of the correlation function

An approximate model for the correlation function can be derived by assuming that the illumination over the interrogation spot, I_o, is constant, and then substituting the previously derived equation for the particle image intensity into Eq. (38). (This model of the correlation function is approximate in that its accuracy depends on the model of the particle image intensity function.) First, assuming that the particle image intensitiy function is given by $I = I_o\hat{J}_o$, the following result is obtained

$$\hat{J}_o[\mathbf{X};z] = \frac{f(z)}{I_o}\exp\left(\frac{-4\beta^2(X^2+Y^2)}{d_e^2(z)}\right) \tag{41}$$

where $f(z) = \frac{J_P D_a^2 \beta^2}{4\pi d_e^2(z)(\mathbf{s}_o+z)^2}$, and $d_e(z)$ is given by Eq. (3). Equation (38) can be solved by making the simplifying assumption that Δz is small, either by making the velocity in the z direction small or by setting Δt small enough that the particles do not move very far in the z direction. The weighting function in Eq. (40) can then be expressed as

$$W(\mathbf{x}) = \frac{C(\mathbf{x},t)W_{I1}(M\mathbf{x}-\mathbf{X_1})W_{I2}(M\mathbf{x}+M\Delta\mathbf{x}-\mathbf{X_2})}{d_e^4(z)(\mathbf{s}_o+z)^4} \tag{42}$$

Note that for $M \gg 1$, the parameter d_e/M is almost independent of M. The dimensionless weighting function $W(x)M^4\mathbf{s}_o^4/d_e^4(0)$ is plotted in Fig. 6 as a function of distance from the object plane using various numerical apertures with 1-μm diameter seed particles and for $\mathbf{s}_o \gg z$.

The weighting function can be used to put a bounds on the interrogation volume in the z direction by defining a distance from the object plane beyond which particles no longer significantly contribute to the correlation function. The contribution of a particle to the correlation function can be said to be insignificant when the ratio of its weighting function to the weighting function of a particle at $z = 0$ falls below some threshold. This threshold is defined by the parameter ε. If the concentration of seed particles is assumed to be constant throughout the interrogation volume, to find z_{corr}, first assume that $s_o \gg z$, and then solve the equation

$$\varepsilon = \frac{d_e^4(0)}{d_e^4(z_{corr})} = \frac{\left(M^2d_p^2 + 5.95(M+1)^2\lambda^2 f^{\#2}\right)^2}{\left(M^2d_p^2 + 5.95(M+1)^2\lambda^2 f^{\#2} + \frac{M^2 z_{corr}^2}{f^{\#2}}\right)^2} \tag{43}$$

which yields the result

$$z_{corr} = \left[\frac{(1-\sqrt{\varepsilon})}{\sqrt{\varepsilon}}\left(f^{\#2}d_p^2 + \frac{5.95(M+1)^2\lambda^2 f^{\#4}}{M^2}\right)\right]^{1/2} \tag{44}$$

An experimental parameter, the *depth of correlation*, first introduced by Wereley et al. (2000), can then be defined as the depth over which particles significantly contribute to the correlation function. This depth would simply be $2z_{corr}$.

Using Eq. (44), for a μPIV experiment with NA = 0.5 ($f^{\#} = 1.0$), $d_p = 1$ μm, $M = 20$, $\lambda = 0.56$ μm, and $\varepsilon = 0.01$, the distance from the object plane beyond which the contribution becomes insignificant, z_{corr}, would be 5.25 μm. The depth of correlation would thus be 10.5 μm. Note that for this objective, $\mathbf{s}_o \cong f = 9$ mm, so the assumption that $\mathbf{s}_o \gg z$ is excellent. Table 1 contains information on the depth of correlation for a number of objectives and particle diameters with $\varepsilon = 0.01$. Following the analysis of Wereley et al. (1999), we found that $\varepsilon = 0.01$ is a reasonable choice. Additionally, z_{corr} is approximately proportional to $\varepsilon^{1/4}$, and as such, is not strongly affected by small changes in the choice of ε.

Depth of correlation is seen to be only weakly dependent on the magnification. The depth of correlation can be

Table 1. Depth of correlation for various objectives and particle diameters

M	NA	d_p [μm]	$2z_{corr}$ [μm]
10	0.25	0.5	36.6
10	0.25	1.0	38.0
20	0.5	0.5	9.1
20	0.5	1.0	10.5
40	0.6	0.5	6.3
40	0.6	1.0	7.7
60	0.8	0.5	3.8
60	0.8	1.0	5.0

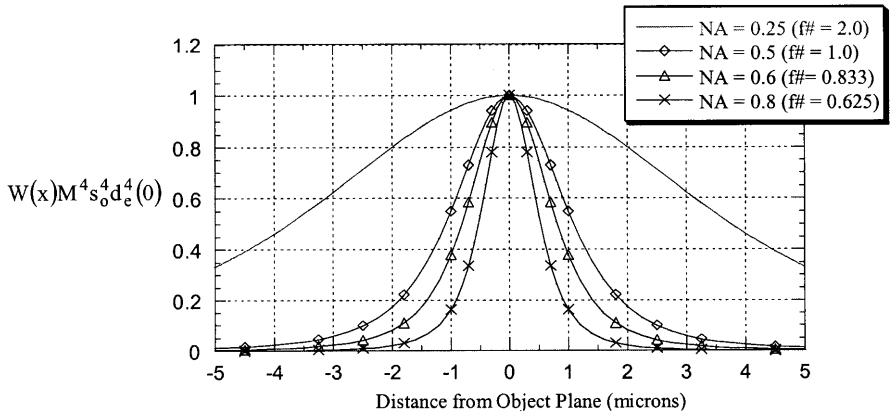

Fig. 6. Correlation weighting function for various numerical apertures with 1-micron particles

most easily adjusted by changing the $f^{\#}$ (or the numerical aperture). The depth of correlation increases approximately linearly with $f^{\#}$ for large particles (particles for which the geometric optics term dominates image diameter) and increases approximately with the square of $f^{\#}$ for small particles (particles for which the diffraction term dominates image diameter).

5 Summary and conclusions

Microscopic PIV differs from traditional PIV in that instead of illuminating only a thin sheet of particles with a light sheet, all the particles in the flowfield are illuminated, and the depth over which particle images can be seen is dependent on the optics of the system. This results in some problems unique to μPIV. The first is that the diameter and intensity of a particle image are dependent on distance from the object plane. The second is that those particles far from the object plane form a background glow that can make it difficult to see the near-focus particles. To address these problems, an approximation for the particle image intensity function has been formulated, and a new parameter, particle visibility, has been introduced. Particle visibility is found to be dependent on the focal number of the system and only weakly dependent on the magnification. Other parameters that can effect particle visibility are the depth of the microfluidic device, the diameter of seed particles used, and the concentration of seed particles.

General equations describing the conditionally averaged cross-correlation function for a μPIV system have been derived. The particle image intensity function combined with these equations yields insight into how the correlation function, and thus the measured velocity, is affected by various experimental parameters. The measured velocity is found to be a weighted average over the depth of the fluidic device. Integration using the weighting function can be used to determine biasing of the measured velocity due to velocity variation within the interrogation volume.

Finally, the weighting function has been used to put a bound on the interrogation volume in the z direction by defining a distance from the object plane beyond which particles no longer significantly contribute to the correlation function. An experimental parameter, the depth of correlation, was then introduced that defines the bounds on the interrogation volume in the z direction. The depth of correlation is found to be dependent on the focal number of the optical system. For large seed particles, the depth of correlation is approximately proportional to $f^{\#}$, and for small seed particles the depth of correlation is approximately proportional to $f^{\#2}$.

References

Adrian RJ (1986a) An image shifting technique to resolve directional ambiguity in double-pulsed velocimetry. Appl Optics 25: 3855–3858

Adrian RJ (1986b) Statistical properties of particle image velocimetry measurements in turbulent flow. In: Asanuma T, et al (eds) Applications of Laser Anemometry to Fluid Mechanics, Ladoan Lisbon, pp 115–129

Adrian RJ (1991) Particle-imaging techniques for experimental fluid mechanics. Ann Rev Fluid Mech 23: 261–304

Adrian RJ; Yao CS (1983) Development of pulsed laser velocimetry measurement of fluid flow. In: Univ Missouri Rolla, pp Symp on Turbulence

Adrian RJ; Yao CS (1985) Pulsed laser technique application to liquid and gaseous flows and the scattering power of seed materials. Appl Optics 24: 42–52

Barnhart DH; Adrian RJ; Papen GC (1994) Phase conjugate holographic system for high resolution particle image velocimetry. Appl Optics 33: 7159–7170

Keane RD; Adrian RJ (1990) Optimization of particle image velocimeters: I. Double pulsed systems. Meas Sci Technol 1: 1202–1215

Keane RD; Adrian RJ (1991) Optimization of particle image velocimeters: II. Multiple pulsed systems. Meas Sci Technol 2: 963–974

Keane RD; Adrian RJ (1992) Theory of Cross-Correlation of PIV images. Applied Scientific Research 49: 191–215

Meinhart CD; Wereley ST; Santiago JG (1999) Micro-resolution velocimetry techniques. In: Adrian RJ, et al (eds) Developments in Laser Techniques and Applications to Fluid Mechanics. Springer, Berlin Heidelberg New York

Meinhart CD; Wereley ST; Gray MHB (2000) Volume illumination for two-dimensional particle image velocimetry. Meas Sci Technol 11: 809–814

Meng H; Hussain F (1995) In-line recording and off-axis viewing technique for holographic particle velocimetry. Appl Optics 34: 1827–1840

Santiago JG; Wereley ST; Meinhart CD; Beebe DJ; Adrian RJ (1998) A particle image velocimetry system for microfluidics. Exp Fluids 25: 316–319